Science of the Total Environment 1001 (2025) 180565

Contents lists available at ScienceDirect

Science of the Total Environment

journal homepage: www.elsevier.com/locate/scitotenv

Indicators of carbon alteration (ICAs) suggest patterns in reservoir methane emissions

H.I. Jager [a,b,*], R.M. Pilla [a], A. Cardall [c], C.H. Hansen [a], P.G. Matson [a], N.A. Griffiths [a]

[a] Oak Ridge National Laboratory, Oak Ridge, 37831-6038, TN, USA
[b] Current address: University of Tennessee, Knoxville, 37914, TN, USA
[c] Brigham Young University, Provo, UT, USA

HIGHLIGHTS

- Indicators of carbon alteration, ICAs, stand in for complex models & measurements.
- We calculated ICAs for three reservoirs in the Tennessee River basin.
- ICA's quantified four causal pathways to methane emissions from available data.
- ICA-suggested longitudinal patterns in emissions require further testing.
- ICA-suggested seasonal patterns have implications for reservoir operations.

GRAPHICAL ABSTRACT

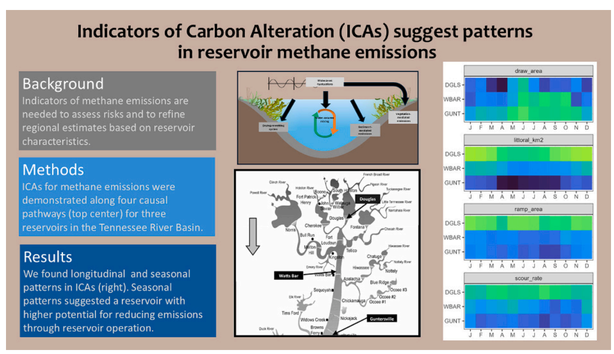

ARTICLE INFO

Keywords:
Methane
Greenhouse gases
Reservoir cascade
Hydropower reservoirs
Indicators of carbon alteration (ICA)

ABSTRACT

Reservoir operations influence emissions via multiple causal pathways. In this paper, we quantify indicators of carbon alteration (ICAs) focused on methane. ICAs were chosen to reflect the potential for methane emission along four causal pathways: 1) water column mixing, 2) wet-dry cycles in sediment, 3) sediment redistribution, and 4) vegetation. We developed algorithms to calculate ICAs for three reservoirs along a longitudinal gradient in the Tennessee River basin of the southeast US. The ICAs revealed interesting longitudinal patterns. Indicators of both methane production and destruction increased downstream. The potential for ebullitive methane emissions driven by sub-daily water level fluctuations and emissions mediated by vegetation were higher in downstream mainstem reservoirs than in the upstream tributary reservoir. Along the remaining two pathways, longitudinal patterns were equivocal (sediment pathway) or suggested decreased emissions downstream (water-column mixing). We also observed seasonal patterns and, by combining ICAs, inferred times when ramping could be achieved with lower risk of emissions. The ICAs demonstrated here are the first step in quantifying mechanistic relationships between reservoir operation and methane emissions. In future, they may lead to improved operations in reservoir cascades and regional-scale estimates of emissions that account for differences among reservoirs.

* Corresponding author at: University of Tennessee, Knoxville, TN, 37914, USA.
E-mail address: hjager@utk.edu (H.I. Jager).

https://doi.org/10.1016/j.scitotenv.2025.180565
Received 2 May 2025; Received in revised form 5 September 2025; Accepted 18 September 2025

1. Introduction

Greenhouse-gas (GHG) emissions from freshwater systems are a growing concern (Rodriguez et al., 2018; Saunois et al., 2016). The contribution of hydropower reservoirs to global GHG emissions is highly uncertain (Hansen et al., 2025) and existing methods for estimating emissions from individual reservoirs at regional scales are limited. For example, Tier 1 and 2 methods adopted by the IPCC rely on crude estimates of areal emissions factors for entire countries (IPCC, 2006) multiplied by estimates of surface area that are also highly variable (Hansen et al., 2022).

GHG emissions from water bodies with managed flow releases, i.e., reservoirs, are of interest because they can potentially be reduced. Typically, hydropower reservoirs are built in cascades because hydropower can be generated from the same parcel of water multiple times as it moves downstream. Yet, only a few studies have compared longitudinal patterns in methane emissions, mostly in large rivers of China (Liu et al., 2020; Liu et al., 2016; Zhong et al., 2023). In the Upper Mekong, methane production in sediments increased downstream (Liu et al., 2020). In the Luanhe River, water elevation (depth) controlled methane emissions in deeper reservoirs, whereas primary production was found to be more important in the shallower downstream reservoir (Zhong et al., 2023),

Indicators are one class of research tool used to quantify human influence (such as GHG emissions) (Heink and Kowarik, 2010). Indicators are used by national (e.g., US Environmental Protection Agency) and International (IPCC, 2006) government entities to produce regional and global scale estimates of emissions because detailed measurement and modeling are not feasible. Useful indicators are: 1) easily understood by laypersons, 2) quantitative and easy to calculate or measure, 3) acceptable in terms of implementation cost (data collection, calculation), 4) relevant to a specific management context, but also broadly applicable to allow comparisons (e.g., among waterbodies or between time periods), 5) sensitive to changes of interest, and 6) scientifically justifiable. Ideally, environmental indicators should be easy to measure or model and have a close relationship to the causal factor of interest (Laura et al., 2000). For example, indicators of Hydrologic Alteration (IHA) were introduced as a way to quantify the effects of river regulation on flow regimes (Richter et al., 1996), and have successfully been used in a wide range of studies to quantify the effects of river regulation (Eng et al., 2017; Homa et al., 2013; McManamay et al., 2022). When combined with indices of biotic integrity, IHAs have been used to evaluate ecological responses to hydrologic alterations (Boavida et al., 2020; Jumani et al., 2018).

The successful use of IHAs to understand anthropogenic alterations suggests that Indicators of Carbon Alteration (ICA) could be used in a similar manner to guide reservoir management toward reduced GHG emissions, for example, through changes in the timing of water releases. Although our understanding of how flow releases influence GHG emissions is far from complete, a few studies have measured changes in GHG emissions before and after significant water releases during reservoir drawdown (Beaulieu et al., 2018; Deemer and Harrison, 2019; Harrison et al., 2017).

We focus here on methane, which accounts for a significant fraction of radiative forcing from reservoirs (Soued et al., 2022). Methane has a high global warming potential compared to CO_2. Unlike CO_2, methane emissions can be attributed to reservoir creation and operation (Prairie et al., 2018). Whereas carbon will return to the atmosphere as CO_2 regardless of whether it passed through algae (Prairie et al., 2018) or where it was transported, conditions for producing and emitting methane can be modified by human activity (Jager et al., 2022).

We build on previous research focused on methane in which we developed a conceptual model (Fig. 1) to link reservoir water levels to methane emissions (Jager et al., 2023). There, we identified ICAs associated with each of four causal pathways linking water-level fluctuations in reservoirs to methane emissions (water-column mixing, drying-rewetting, sediment delivery and redistribution, and plant-mediated emissions).

In this study, we refined and augmented the initial suite of proposed ICAs for methane (Jager et al., 2023). These were focused on the effects of water-level fluctuations on methane emissions. But, fully understanding emissions also requires considering indicators related to methanogenesis and methanotrophy, processes that create and consume methane, respectively (Fan et al., 2022). Reservoir elevation and depth influences the balance between production and consumption of methane. Microbial communities that produce methane tend to dominate in warm, shallow, and permanently wetted areas when reservoirs are typically at full pool and methane may be trapped below the thermocline; in contrast, methanotrophs tend to dominate in deeper sediments (Pierangeli et al., 2021; Rey-Sanchez et al., 2019).

Releases of sediment methane to the atmosphere are affected by the timing and amounts of water released at seasonal and diurnal timescales (Jager et al., 2023). At a diurnal timescale, water level fluctuations (WLF) can disrupt reservoir stratification, oxygenating sediments (Kennedy et al., 1985). Along the water-column mixing pathway, we hypothesize that mixing induced by reservoir operation decreases methane emissions (Jager et al., 2023). At a diurnal timescale, drying-rewetting cycles (Maavara et al., 2020) increase dissolved oxygen concentrations in sediment pore water. When oxygen penetrates drying sediments, methanotrophy is promoted and methanogenesis declines (Lyautey et al., 2021). Diurnal fluctuations can also alter hydrostatic pressure, which in turn can affect the release of methane from sediments via ebullition (Beaulieu et al., 2020; Deemer and Harrison, 2019). Field studies have found drawdown events (i.e., ramping) to be important drivers of ebullition (Beaulieu et al., 2018; Harrison et al., 2017; Keller et al., 2021), especially during the inundation phase (Hao et al., 2019; Su et al., 2024). Fast drawdown may also stimulate transport of methane produced in shallow side channels to upper layers of the main reservoir with minimal opportunity for oxidation (Thalasso et al., 2020).

Over an extended time, seasonal drawdown exposes sediments to oxygen, inhibiting production of or consuming methane. Prolonged drawdown has typically been associated with increases in methanotrophs and decreases in methanogens (Tian et al., 2023). The surface area of sediment with anoxic conditions conducive to methane production also declines with drawdown as water retreats toward the main channel and forebay (Hilgert et al., 2019). Whereas the majority of methane is produced and accumulates in deep sediment, the proportion reaching the atmosphere is higher in nearshore areas (Thalasso et al., 2020), and this perimeter area is smaller during drawdown.

The potential for methane generation is decreased by erosion because locally eroded organic carbon is deposited in deeper areas of a reservoir where methane gas produced will be exposed to oxidation while rising through the water column. This quantity can be significant; for example, in tropical water impoundments, nearly 40 % of organic soils were eroded from drawdown zones over ~80 years (Felix-Faure et al., 2019).

Finally, emergent vegetation can transport methane from sediments in the littoral zone through tissues that facilitate gas diffusion in wetland plants called aerenchyma (Bodmer et al., 2024). Methane emissions are estimated to be roughly twice that in vegetated areas compared to unvegetated areas for both methane and CO_2 (Grasset et al., 2025). Reservoir operations may influence the development of littoral communities and, indirectly, vegetative emissions. For example, shoreline vegetation following reservoir inundation recovers much faster in stable reservoirs than in those with large fluctuations (Kaczmarek et al., 2025).

To illustrate the proposed ICAs, we developed algorithms to calculate them for three hydropower reservoirs along a longitudinal gradient (from upstream to downstream) in the southeast US. We see this as a necessary first step toward developing improved Tier-2 national assessments and toward assessing the potential for reducing methane emissions through reservoir operations, i.e., changes in the timing and magnitude of reservoir releases. We end by examining next steps in

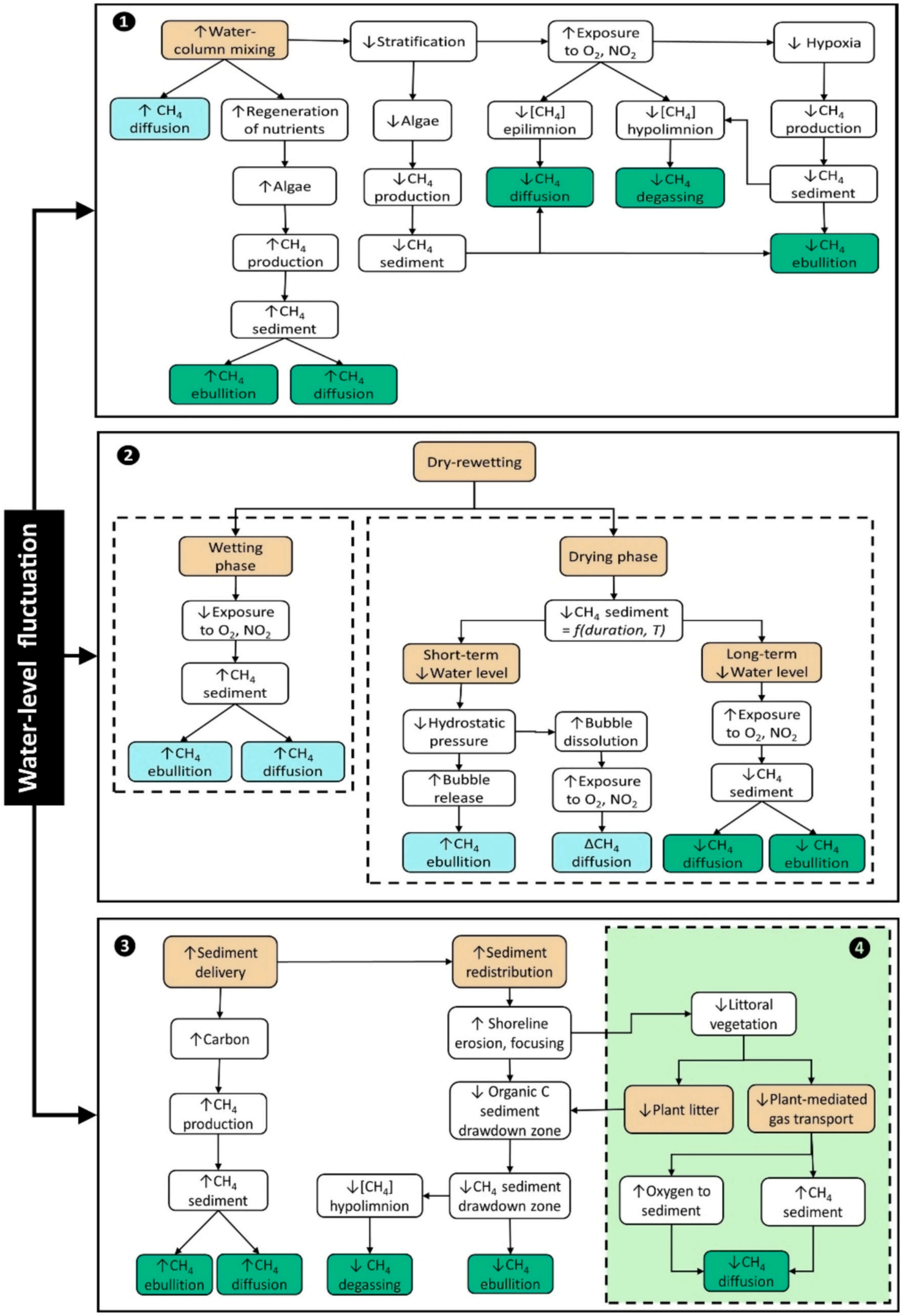

Fig. 1. Causal diagram showing hypothesized linkages between reservoir water-level fluctuations and associated changes in methane emissions via different emission pathways (ebullitive, diffusive, and degassing). Long- (short-) term responses are shown in green (cyan). Used with permission from (Jager et al., 2023).

refining the suite of ICAs.

2. Demonstration of ICAs in southeastern US reservoirs

This study focuses on the southeastern US. Seasonal drawdown begins in autumn in storage reservoirs used for flood control, typically lasting until spring. Drawdown ensures that enough storage capacity is available to store water from high spring flows, water that is later used to fulfill summer water demand. At daily timescales, some hydropower reservoirs are operated to release more water when energy prices are high. The increased release of water during peak, unmet electricity demand results in diurnal fluctuations in water level, 'hydropeaking'.

We modeled three reservoirs (Guntersville, Watts Bar, Douglas) in the Tennessee River basin in the southeastern United States that are operated by the Tennessee Valley Authority, TVA (Fig. 2).

We quantified the proposed ICAs to estimate the effects of reservoir operation on methane emissions at both seasonal and diurnal scales. Quantifying these indicators identified causal pathways that are likely to have the largest positive and negative effects on methane emissions in each reservoir.

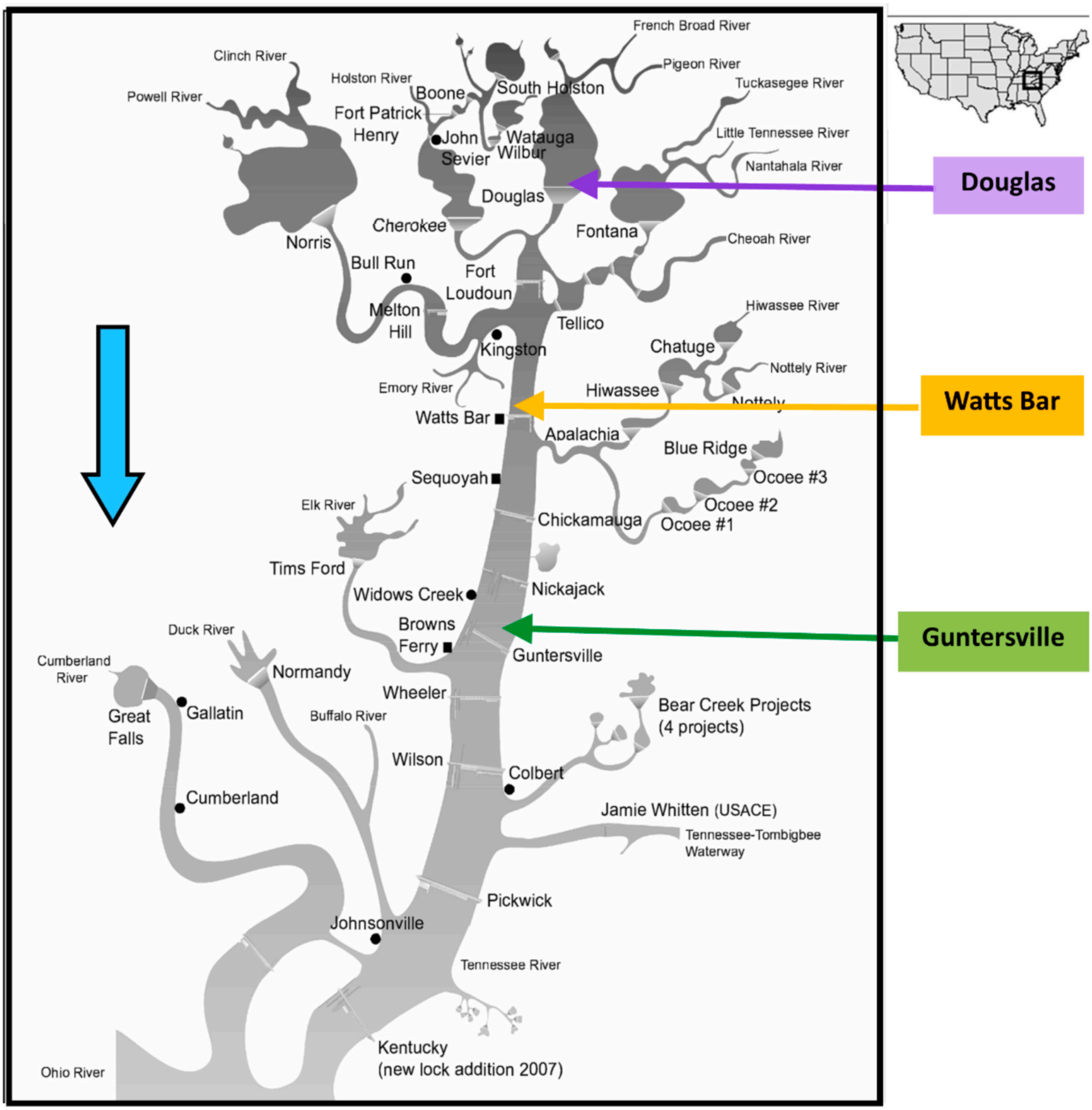

Fig. 2. Schematic diagram of the Tennessee Valley Authority water control system showing three reservoirs of interest. Source: (Tennessee Valley Authority, 2004). The direction of flow toward the Mississippi River is shown by the blue arrow.

3. Methods

3.1. Data

ICAs depended on static and dynamic (i.e., time series) data. Data treated as static for our purposes (due to limited data availability) included bathymetry and light extinction coefficients for each reservoir. To represent bathymetry, we digitized fishing maps produced using SonarChart™ for depth contours at 0, 5, 10, 15, and 20 m for Guntersville and Watts Bar reservoirs, and at 0, 4, 10, 11, 15, and 20 m for Douglas Reservoir (Fig. 3). Light extinction coefficients, k_d, were estimated from photosynthetically active radiation (PAR) measured at depths 0, 0.5, 1, 1.5, and 2 m at six stations per reservoir in 2021–2022 and used to estimate an average Secchi depth. Morphometric and operating characteristics of each reservoir are summarized in Appendix A Table A.1.

Time-series data included sub-daily (15 min) and daily reservoir elevation measurements (used for sub-daily and seasonal ICAs, respectively) for water years 2006 to 2019. Missing values in 2011–12 were imputed (Appendix B). We calculated sub-daily indicators from 15-min elevation and flow releases from the same reservoirs (Dr. Stephen Signore, TVA, personal comm.). Seasonal indicators were estimated from daily reservoir levels, storage volume, and outflows (both turbine releases and total releases) (Steyaert et al., 2022; Wang et al., 2018) over a 20-y period. Typical patterns of seasonal operation are shown in Fig. 4. Douglas Reservoir, impounding the French Broad River, is one of three main tributary reservoirs. Below Douglas, the French Broad River meets the Holston River to form the Tennessee River. Watts Bar Reservoir is on the mainstem Tennessee River below its junctions with two tributaries, the Little Tennessee and Clinch Rivers. Guntersville Reservoir is farther downstream, after the Hiwassee River has joined the mainstem Tennessee River.

Sub-daily indicators required cross-referencing between water elevation and other reservoir dimensions. To simplify this, we developed regression relationships to speed up calculation of reservoir surface area from 15-min (sub-daily) reservoir elevation data (Table A.2). Surface air temperatures were obtained from DAYMET (Thornton et al., 2022) for calculations of degree days and related ICAs.

3.2. Proposed indicators of carbon alteration (ICA)

We implemented a subset of indicators proposed by Jager et al. (2023). Calculations were performed by using the R Statistical Software v4.3–4.4 (R Core Team, 2024). Code can be found at https://github.com/hjager/GHG-indicators. ICAs are described in Table 1.

3.3. Simulating sub-daily indicators

Several sub-daily indicators measure processes leading to hypothesized increases or decreases in methane emissions from shallow sediments (Fig. 1, Table 1). For each reservoir, we report the medians of values for each 15-min period by month and water year.

Diurnal changes in wetted area along the reservoir perimeter are especially relevant to the production and consumption of methane, and this requires estimating perimeter from reservoir bathymetry as a function of the daily change in reservoir elevation. For each 15-min interval within a given day, we used log-linear interpolation to estimate elevations between digitized contours and retrieved the perimeter (i.e., length) of the associated contour. To estimate wetted perimeter area, we integrated the log-perimeter between the daily low and high elevations using the trapezoidal rule from calculus and then back-transformed the result to obtain area in km^2 (*ramp_area*). We confirmed that the algorithm converged as the change in elevation decreased and then used 10^{-5} m as the interval. We assumed that the slope from the upper layers continued to estimate areas below the deepest digitized depth.

The sub-daily indicator *ramp_vol_frac* measures daily turnover in the volume of water and is most relevant to the water-column pathway to methane emissions (Fig. 1a). When *ramp_vol_frac* is high, the opportunity for thermal stratification in summer is lower. The resulting mixing of water layers brings oxygenated water deeper, moderating temperatures across the water column. Despite higher bottom temperatures, empirical evidence suggests that the net result of mixing is lower production in sediments due to increased oxygenation (Guérin et al., 2016). Therefore, *ramp_vol_frac* in summer should be negatively correlated with methane production. Unlike wetted perimeter, it was easy to estimate the relative change in volume (*ramp_vol_frac*) from the extremes in daily volume (Eq. (1)).

$$ramp\_vol\_frac = \frac{(Vmax - Vmin)}{Vmax} \tag{1}$$

where

$Vmax$ = maximum daily volume

$Vmin$ = minimum daily volume

Similarly, the minimum and maximum within-day reservoir elevations and their times were used to characterize the duration of increases (*rise_duration*) or decreases (*drop_duration*) in elevation in h, depending on whether the maximum daily elevation occurred before or after the minimum daily elevation (Eq. (2)).

$$drop\_duration = Hmin - Hmax, Hmax \leq Hmin,$$

$$rise\_duration = Hmax - Hmin, Hmax > Hmin,$$

$$where: \tag{2}$$

$Emax$ = maximum daily elevation,

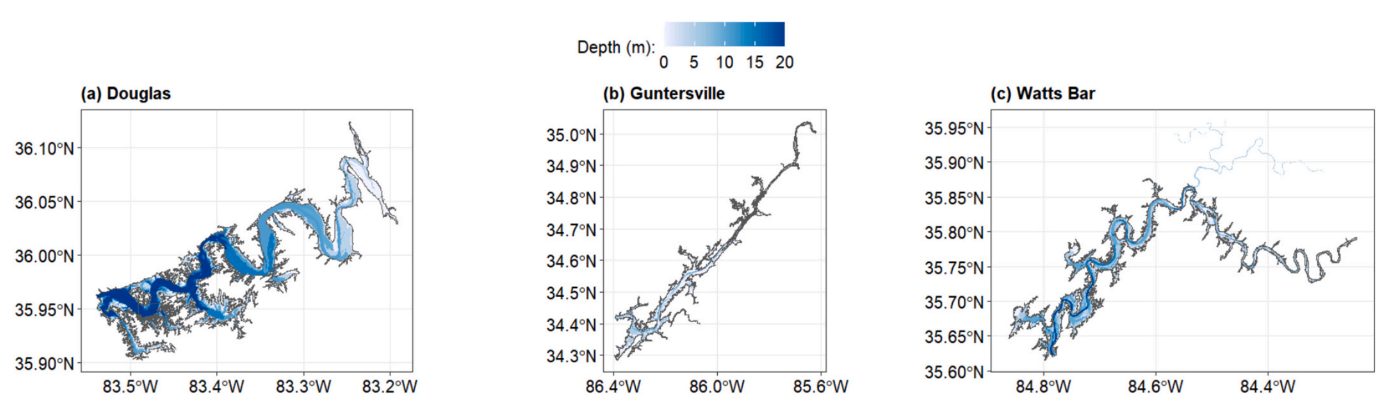

Fig. 3. Bathymetry for each of the three study reservoirs, a) Douglas, b) Guntersville, and c) Watts Bar.

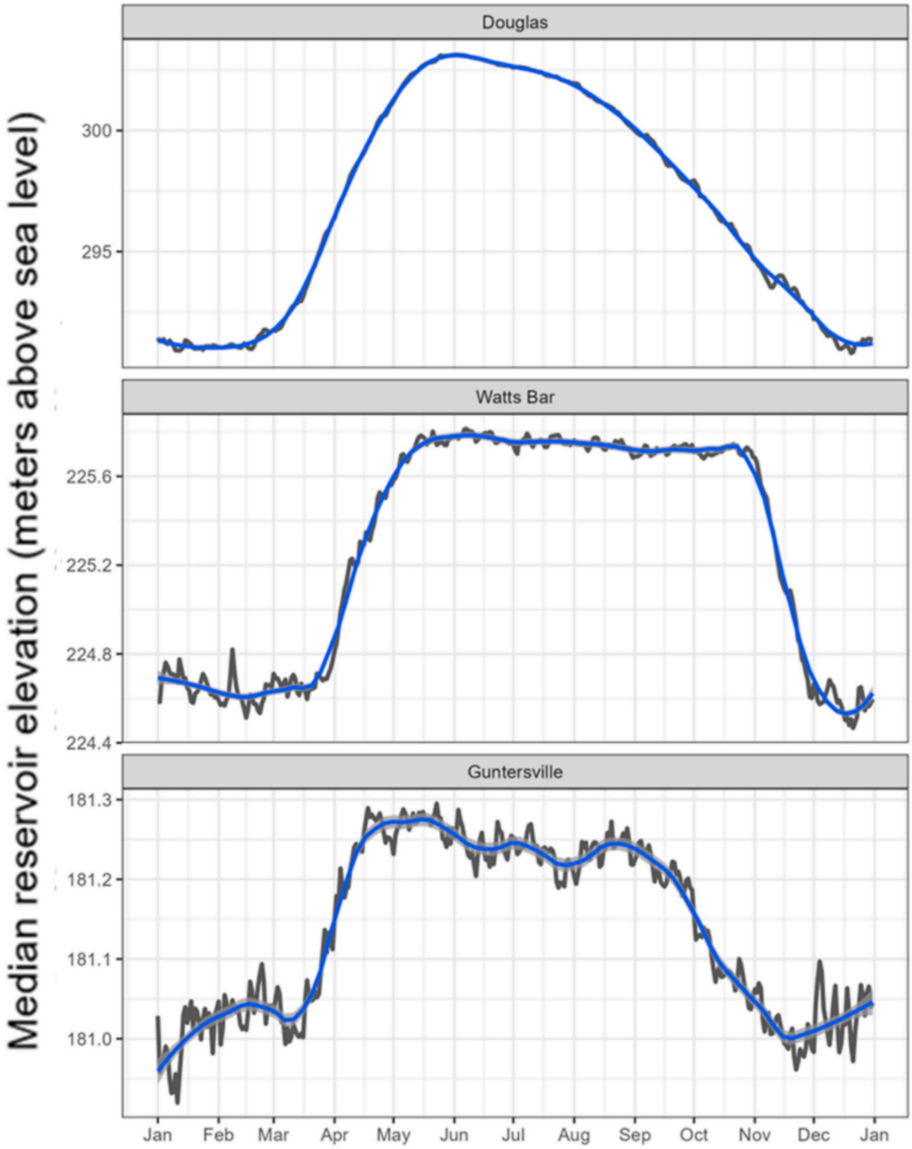

Fig. 4. Smoothed (blue) and unsmoothed (grey) median daily reservoir elevations showing seasonal patterns and short-term fluctuations over the period 2005–2022. Graphs have different scales with much lower variability in the downstream reservoirs, Watts Bar and Guntersville.

Emin = minimum daily elevation,

H = time of *Emin* or *Emax* in h

The rate of decrease in elevation (*efall_rate*) was also calculated from these reference values (Eq. (3)).

$$Efall_{rate} = \frac{Emax - Emin}{Hmax - Hmin}, Hmax < Hmin \quad (3)$$

Scour rate (*scour_rate*, Eq. (4)) is an indicator of sediment focusing that can result in decreased emissions, as discussed in Jager et al. (2023).

$$scour\_rate = Efall\ rate \left(\frac{Nrev}{2}\right) \quad (4)$$

The number of elevation reversals (*Nrev*) was calculated by counting changes in the sign of elevation differences between adjacent 15-min intervals each day, with a total of 24 × 4–1. We excluded changes smaller than 5 % of *Efall_rate*.

3.4. Simulating seasonal ICAs

Seasonal indicators were defined for each water year (Oct 1 to Sept 30) (Tennessee Valley Authority, 2004) and reservoir based on daily time series of reservoir elevations (elevation, m), surface area (area, m^2), and storage volume (volume, m^3).

To reach the atmosphere, methane generated in sediments must avoid oxidation while rising through the water column, an event that is more likely in shallow areas. Indicators that quantify seasonal changes in wetted littoral area are therefore relevant to understanding the effects of shallow water on emissions. We estimated littoral area on each day as the wetted area below the surface elevation where light can still penetrate. Secchi depth (m), which estimates the photic layer with light intensity of 1 % (Schindler, 1971) was estimated from the eq. 1.7 / k_d (Wetzel, 1983). An annual average from 1 to 3 field campaigns ($n = 6$ sites per reservoir per campaign) was used to estimate the depth of the photic zone of each reservoir (Table A.1).

We characterized drawdown area (*draw_area*) from bathymetry and daily reservoir elevation as described in Section 3.3 for sub-daily indicators (Table 1). *Draw_area* estimates the area of sediment affected by

Table 1
Indicators of carbon alteration (ICAs) focused on methane. Run-based indicators are annual summaries of seasonal patterns.
The hypothesized direction of the ICA relationship with methane emissions is shown as positive (↑), negative (↓), or neutral (no arrow). Justification for most ICAs below can be found in (Jager et al., 2023). WY = water year.

Acronym	Description	Units	1. Water-column mixing	2. Dry-re-wetting cycles	3. Sedi-ment redistr.	4. Littoral vegeta-tion	Temporal extent (output)	Temporal resolution (input data)
Sub-daily and seasonal indicators								
Aspect_ratio	Ratio of water surface area in littoral zone [defined by Secchi depth] to total water surface area at full pool].	None				↑	Seasonal (month, WY)	Daily elevation
Draw_area	Sediment surface area between monthly min. and max. elevation.	km^2			↓		Seasonal (month, WY)	Daily elevation
Efall_rate	Within-day rate of decrease in elevation	m / h		↑	See scour_rate		Subdaily (month, WY)	Subdaily elevation
Littoral_km2	Water surface area within the photic zone based on Secchi depth	km^2				↑	Subdaily (month, WY)	Subdaily elevation
Nrev	Daily reversals in reservoir elevation >5 % of daily change	#			See scour_rate		Subdaily (month, WY)	Subdaily elevation
Ramp_area	Sediment surface area exposed to max. within-day change in elevation	km^2	See ch4_prod	↑	↓		Subdaily (month, WY)	Subdaily elevation
Ramp_vol_frac	Fraction of water volume turned over within a day	None	↓				Subdaily (month, WY)	Subdaily elevation
Scour_rate	Product of within-day Efall_rate and Nrev/2	# • m / h			↓		Subdaily (month, WY)	Subdaily elevation
Run-based indicators associated with full-pool and drawdown periods								
Draw_dur	Duration of drawdown (longest run of days below median elevation)	d			↓		Seasonal (WY)	Daily elevation
Fpool_dur	Duration of fullpool (longest run of days above median elevation)	d	↑			↓	Seasonal (WY)	Daily elevation
Fpool_Q10	Cumulative degree days during full pool	° C-d	NA	NA	NA	NA	Seasonal (WY)	Daily elevation
CH4_prod	Fpool_Q10 x Ramp_area	km^2 -°C d	↑	↑	↑	↑	Seasonal (WY)	Daily elevation

the maximum change in elevation experienced during the period of interest (i.e., month).

The seasonal indicator, *aspect_ratio*, measures the proportion of water surface area in shallow areas. Because temperature is higher near the surface, methane production tends to be higher in shallow areas. Further, methane emissions are correlated with transport of water from shallow areas to deep areas (Encinas Fernández et al., 2016). We estimated *aspect_ratio* as the mean ratio of shallow water area (i.e., littoral area) to maximum surface area at full pool. Shallow-water surface area was estimated as the difference (i.e., outer ring) between the reservoir surface area on each day and the surface area estimated at the depth of the photic zone divided by total surface area at full pool elevation (Encinas Fernández et al., 2016). We used the average Secchi depth to estimate both littoral area (*littoral_km2*) and aspect ratio. Surface areas were estimated by using reservoir-specific quadratic regressions with daily depth (Table A.2). Seasonal ICAs were summarized as monthly medians.

3.5. Simulating indicators of methanogenesis and methanotrophy

The remaining seasonal indicators are 'run-based' indicators that measure cumulative metrics of methane production over periods of seasonal drawdown and full pool by water year (Table 1). To calculate these indicators, we partitioned annual reservoir elevation data into runs of consecutive days above and below the median annual elevation, Ec_k, by water year (numbered 1 to 365 from Oct 1 to Sept 30). We defined full pool and drawdown periods as the longest runs above and below median elevation, *Ec*, in each water year, respectively, within the appropriate period (after day 230 for autumn drawdown and before day 180 for spring refill). From these two runs, we defined indicators including durations of drawdown (*draw_dur*) and fullpool (*fpool_dur*), and Julian start and end dates for each period. Differences in the timing and duration of refill and drawdown periods among reservoirs and water years are shown by a Cleveland plot (Appendix C. Fig. S1.1).

We developed methods for incorporating temperature into indicators of methane production, recognizing that the effect of water-level fluctuations is amplified by higher temperatures and dampened by lower temperatures. For simplicity and due to greater daily-scale data availability, we used air, rather than reservoir water temperatures (see Section 3.1 Data). The metric *fpool_Q10* quantifies the thermal production rate for methane using parameters from the WETMETH model (Nzotungicimpaye et al., 2021). For a given water year, Eq. (5) sums a daily Q10 function over days, *k*, across the longest run of reservoir elevations at full pool.

$$fpool\_Q10 = \sum\nolimits_k Q_{10}^{\frac{(T_k - 273.15)}{10}} \quad (5)$$

Next, we developed an index of methane production that measures the longest period (d) of continuously wetted area with warm temperature. *CH4_prod* is a convolution of *fpool_Q10* with daily ramping area along the reservoir's perimeter, *A*, on day *k* (Eq. (6)). Thermal potential for methane production (*ch4_prod*) occurs when high temperatures (indicated by *fpool_Q10*), full-pool duration (*fpool_dur*), and recently inundated or drained area (*ramp_area,* a sub-daily ICA) coincide.

$$CH4\_prod = \sum\nolimits_k |A_k| Q_{10}^{\frac{(T_k - 273.15)}{10}} \quad (6)$$

3.6. Scales of variation in ICAs

We conducted an analysis of variance (ANOVA) to compare variation among months and among water years in monthly-summarized data using a fixed-effect model, ICA = A + B × water year + C × month. For each reservoir and indicator, the ratio of the mean sum of squares and residual mean sum of squares was tested as an F-statistic, with $p < 0.05$ considered statistically significant. In addition, we calculated pairwise correlations between ICAs.

4. Results

We summarized the 'run-based' indicators associated with methane production and consumption. These are accumulated over days within periods of each water year. Next, we present seasonal patterns in both sub-daily and seasonal indicators associated with each pathway linking reservoir operations with methane emissions. Below, Table 2 summarizes all indicators for each reservoir**.**

We compared variation among months and among water years using ANOVA. Among the reservoirs, the magnitudes (y-axis) of effects at both scales, measured by the F-statistic, tended to increase downstream (Appendix C. Table S.2.1).

4.1. Indicators of methanogenesis and methanotrophy

Thermal potential for methane production (*ch4_prod*) occurs when high temperatures (indicated by *fpool_Q10*), full-pool duration (*fpool_dur*), and recently inundated or drained area (*ramp_area,* a sub-daily ICA) coincide. Annual ICAs associated with production and consumption were positively correlated in Guntersville (0.44) and Douglas (0.22), but uncorrelated in Watts Bar Reservoir (0.02). Both ICAs were negatively correlated with water year across reservoirs. More-prolonged methanogenesis (*ch4_prod*) during summer full pool may be offset by more-prolonged opportunities for methanotrophy during seasonal drawdown (*draw_dur*).

Our results showed longitudinal patterns in ICAs for both production and consumption of methane. The ICA for methane consumption (*draw_dur*) decreased downstream (Fig. 5**;** Table 3). For production, some years had extremely high values in Douglas (Fig. 5)**,** but the median *ch4_prod* was lowest upstream in Douglas Reservoir and higher downstream in the mainstem reservoirs (Table 3). Likely, this is because *ch4_prod* is a composite indicator that incorporates *ramp_area*, which increases downstream.

Methanogenesis and methanotrophy determine the quantity of methane subject to influences by reservoir operations via the four causal pathways described below.

4.2. Water-column mixing

When the daily turnover in the volume of water, *ramp_vol_frac*, is high, oxygenated water will reach farther down to sediments, preventing anoxic conditions needed for methane production in summer and promoting methanotrophy. This implies an inverse correlation between *ramp_vol_frac* and summer methane emissions. Note that we focused on changes in volume rather than sediment perimeter, as perimeter is more relevant to other pathways (e.g., dry-rewetting cycles).

During summer full-pool conditions, *ramp_vol_frac* values were lowest in the tributary reservoir (Douglas) and increased downstream (Fig. 6). Seasonal patterns in downstream reservoirs were also weaker than those in Douglas Reservoir. In Douglas Reservoir, the lowest values of *ramp_vol_frac* (highest emissions potential) occurred during full pool (Fig. 6). *Ramp_vol_frac* increased through summer, offsetting a portion of summer methane production. The thermal opportunity for methane production in Douglas Reservoir was higher in earlier years than in later years (Fig. 5).

Table 2

Median (interquartile range) values of indicators of carbon alteration (ICAs) focused on methane across full time series. Summaries for run-based indicators are across water years, and the rest are across days for the full time series. Directions of influence for four pathways (water column, dry-wet cycles, sediment, and vegetation) are positive (↑), negative (↓), or neutral (x). See Table 1 for details about each ICA.

Acronym	Description	Influence	Units	Douglas	Watts Bar	Guntersville
Aspect_ratio	Ratio of water surface area in littoral zone [defined by Secchi depth] to total water surface area at full pool.	↑ x x x	None	0.106 (0.096–0.116)	0.133 (0.129–0.134)	0.203 (0.201–0.204)
CH4_prod	Fpool_Q10 x Ramp_area	↑↑↑↑	km^2 - °C d	260.03 (179.29–20,869.5)	400.5435 (0.12–2837.2)	367.98 (130.12–11,528)
Draw_area	Sediment surface area between monthly minimum and maximum elevation.	x x ↓ x	km^2	1.096 (0.592–1.794)	0.534 (0.288–0.916)	0.367 (0.292–0.498)
Draw_dur	Duration of drawdown (longest run of days below median elevation)	x x ↓ x	D	158.5 (128.75–180.75)	113.0 (74.0–163.0)	49.0 (41.0–61.5)
Efall_rate	Within-day rate of decrease in elevation	x ↑↓ x	m / h	0.0086 (0.007–0.010)	0.0094 (0.007–0.012)	0.0088 (0.007–0.011)
Fpool_dur	Duration of full pool conditions (longest run of days above median elevation)	x ↑ x x	D	170.5 (152.0–188.0)	112.0 (45.25–132.25)	32.0 (24.5–79.0)
Fpool_Q10	Cumulative degree days during the longest run of high-elevation days (i.e., full pool)	↑↑↑↑	°C-d	2989.9 (2828.5–3416.0)	2705.7 (844.84–3056.6)	880.5 (296.3–1393.5)
Littoral_km2	Water surface area within the photic zone based on Secchi depth	x x x ↑	km^2	12.67 (11.52–13.98)	18.05 (17.43–18.17)	53.85 (53.47–54.15)
Nrev	Reversals in reservoir elevation per day exceeding 5 % of daily change (out of 24 × 4–1 possible)	x x ↓ x	#	2.0 (0.0–6.25)	13.2 (4.75–22.0)	20.0 (16.0–24.0)
Ramp_area	Sediment surface area affected by maximum within-day change in elevation	x ↑ ↓ x	km^2	0.0542 (0.041–0.072)	0.1169 (0.100–0.134)	0.1263 (0.108–0.150)
Ramp_vol_frac	Fraction of water volume turned over within a day	↓ x x x	None	0.00041 (0.00030–0.00058)	0.00054 (0.00047–0.00054)	0.00060 (0.00051–0.00072)
Scour_rate	Product of within-day Efall_rate and Nrev/2 = the number of elevation drops / day	x x ↓ x	# • m / h	0.0067 (0.0–0.0304)	0.0533 (0.022–0.1127)	0.085 (0.0659–0.1115)

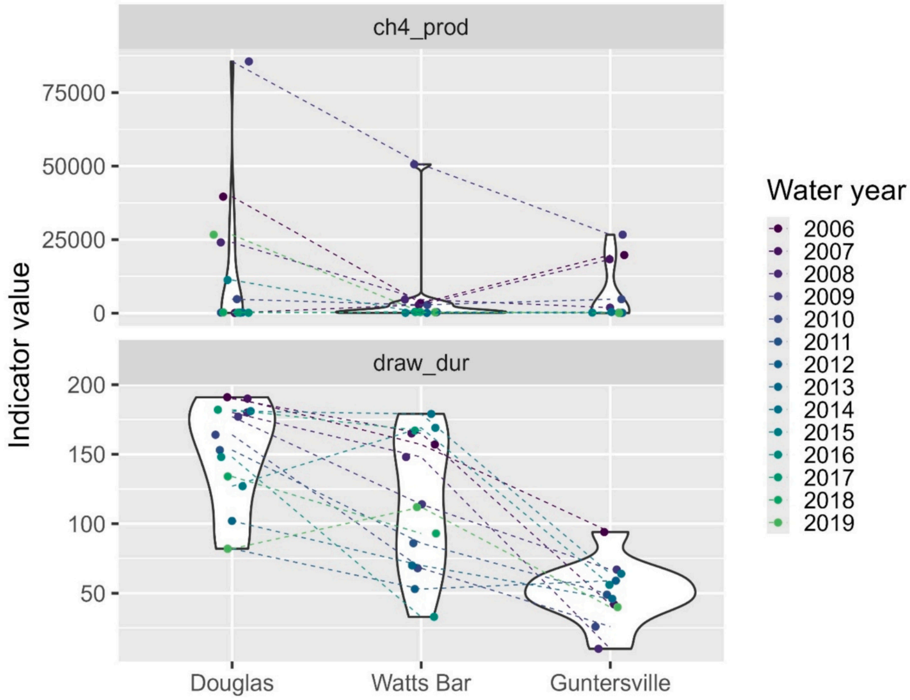

Fig. 5. Violin plots show the distribution of the composite ICA related to methane production [ch4_prod (km^{2} · °C d)] and an ICA related to methane consumption [draw_dur (d)] from water year 2006 to 2019. Quartiles for each reservoir are reported in Table 3.

Table 3
Quartiles of indicators of methanogenesis and methanotrophy and the ratio *draw_dur: CH4_prod.*

Value	Quartile	Douglas	Watts Bar	Guntersville
CH4_prod	0.25	179.29	351.0	130.12
CH4_prod	0.5	260.03	400.5	367.98
CH4_prod	0.75	20,869	2837.2	11,528.0
Draw_dur	0.25	128.75	74.0	41.0
Draw_dur	0.5	158.50	113.0	49.0
Draw_dur	0.75	180.75	163.0	61.5
Ratio	0.25	0.718	0.211	0.315
Ratio	0.5	0.610	0.282	0.133
Ratio	0.75	0.009	0.058	0.005

4.3. Drying-rewetting cycles

Indicators derived from sub-daily data measured shorter-term fluctuations and are especially relevant for methane emissions via ebullition. For example, faster drawdown (a high *efall_rate*) could result in higher potential for ebullition in reservoirs (Fig. 7), especially following a warm season with high methane production (*ch4_prod*) (Aben et al., 2017). The risk of ebullition, indicated by *efall_rate*, was often higher in late summer and early fall than in spring (Fig. 7, top panel).

The area of sediment affected by sub-daily ramping, quantified by *ramp_area*, increased with longitudinal position (Douglas < Watts Bar < Guntersville) (Fig. 7, middle panel). Another sub-daily indicator, *Nrev*, measured the number of short-term fluctuations that rewet sediment (providing limiting nutrients to pores), connect methane in pores to the atmosphere, and then lower hydrostatic pressure (potentially stimulating ebullition) as the water level recedes. *Nrev* was lower in Douglas than in the two downstream reservoirs (Fig. 7, bottom panel). Results suggest that the risk of ebullition, driven by sub-daily water level fluctuations in summer, was higher in Watts Bar and Guntersville reservoirs than in Douglas Reservoir under historical operations.

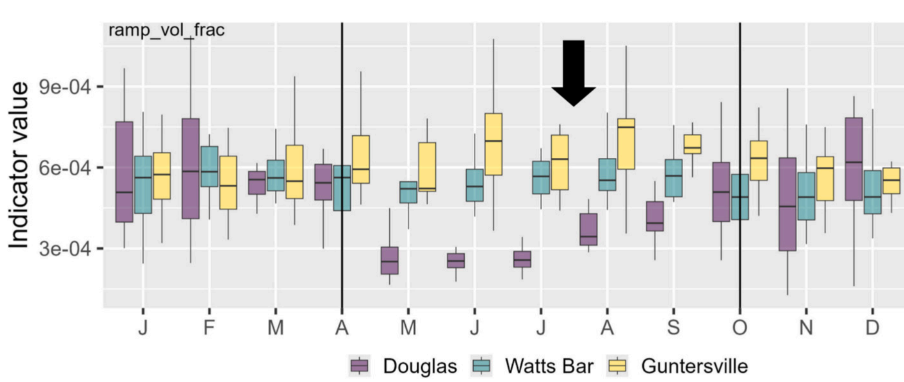

Fig. 6. Indicator ramp_vol_frac measures the daily turnover in volume, an indicator with an inverse relationship with methane emissions via the water-column mixing pathway (black arrow). Longitudinally, Douglas Reservoir is a tributary reservoir that feeds into Watts Bar, which is upstream of Guntersville on the mainstem Tennessee River. Two heavy vertical black bars roughly delimit the period of summer full pool. Boxes enclosing the 25th–75th quartile, a horizontal bar denoting the median among water years, and vertical bars extending to the 5th and 95th percentiles. Outliers are omitted for clarity.

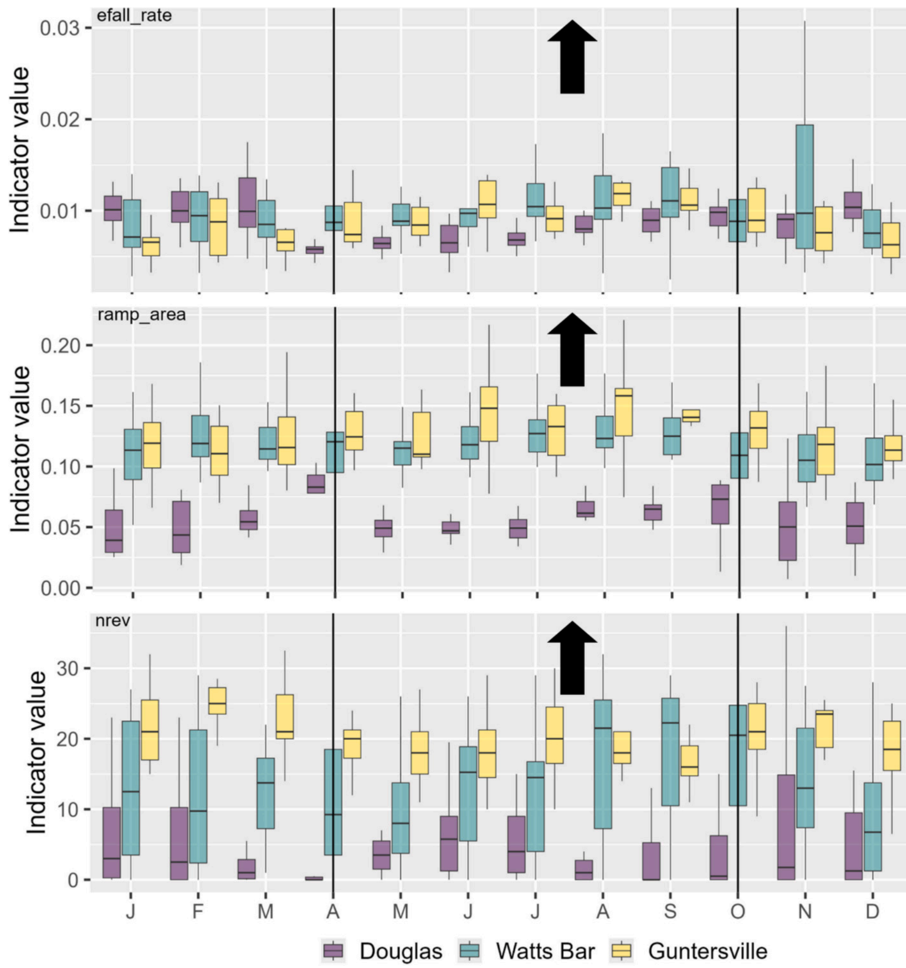

Fig. 7. Three sub-daily indicators hypothesized to have a positive relationship (black arrows) with methane emissions caused by dry-rewetting cycles. Longitudinally, Douglas Reservoir is a tributary reservoir that feeds into Watts Bar, which is upstream of Guntersville on the mainstem Tennessee River. Vertical bars roughly delimit the period of summer full pool. Boxes enclose the 25th–75th quartile, a horizontal bar denoting the median across years and vertical bars extending to the 5th and 95th percentiles. Outliers are omitted for clarity.

4.4. Sediment delivery and redistribution

Two categories of ICAs for emissions associated with sediment are those that measure exposure to erosion and those that measure the erosive forces associated with water-level changes. ICAs related to exposure showed opposite longitudinal patterns at seasonal (*draw_area*, *draw_dur*) and sub-daily (*ramp_area, scour_rate*) timescales. Upstream, Douglas Reservoir experienced the longest seasonal drawdown (*draw_dur*) (Fig. 5) and the most continuously exposed area (*draw_area*) (Fig. 8, top panel).

Erosive forces are captured by scouring rate, *scour_rate*, a compound indicator that combines the number of within-day reversals (*Nrev*) with the within-day rate of decrease in elevation (*efall_*rate). Sub-daily *ramp_area* was higher in the two downstream mainstem reservoirs than in Douglas Reservoir (Fig. 8, middle panel). Values of *scour_rate* also increased downstream, with the lowest values in Douglas Reservoir and highest in Guntersville Reservoir. Seasonally, the three reservoirs experienced the highest values of *scour_rate* in late fall and spring, and the lowest in summer (Fig. 8, bottom panel). Of the three reservoirs, Guntersville is operated with the most stable elevations in the TVA system due to the requirements for navigation (Tennessee Valley Authority, 2004). Although the sub-daily ICAs suggest that short-term fluctuations occur frequently, these fluctuations occur over a narrow band of elevations (Fig. 4).

4.5. Vegetation

Based on the conceptual model (Fig. 1), larger values of morphometric ICAs *littoral_km2* and *aspect_ratio* promote growth of littoral vegetation, leading to a positive association with methane emissions via vegetation. Aspect ratio, a seasonal indicator, measures the proportion of reservoir surface area with depths suitable to support the growth of littoral vegetation whereas littoral area was based on sub-daily measurements. The two ICA's were highly correlated, so using one should suffice (Fig. S2.1).

ICAs related to littoral area pointed to higher emissions in larger downstream reservoirs (i.e., Guntersville) (Fig. 9). This result is intuitive because larger reservoirs should have a larger perimeter and, hence, littoral zone, unless vegetation growth is prevented by steep banks. Our results based on morphometry are consistent with reported patterns in vegetated area, with Guntersville having significant macrophyte coverage throughout much of the reservoir (Tennessee Valley Authority, 2004).

The sediment and vegetation pathways are interconnected. Severe ramping may prevent vegetation from being established, but the rate of erosion is likely higher in areas lacking littoral vegetation. Except for *draw_area*, normalized ICA values show a consistent pattern of higher values in the two downstream reservoirs (Fig. 10).

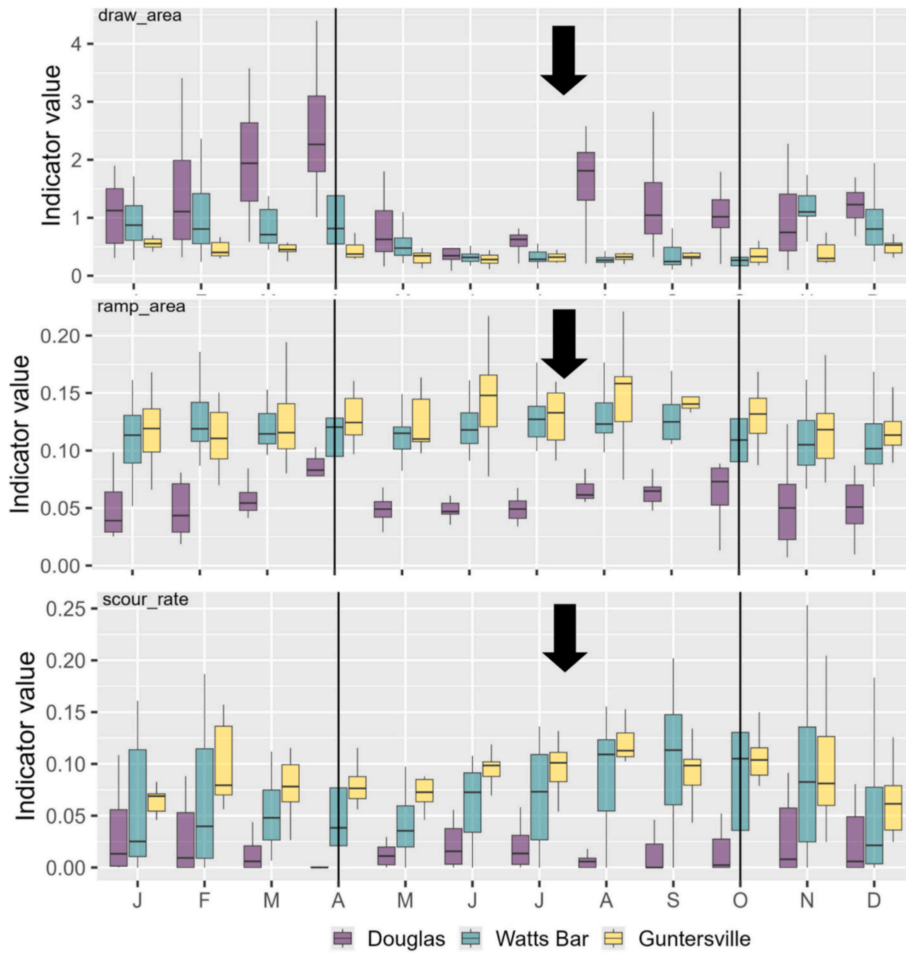

Fig. 8. Indicators hypothesized to have a negative relationship (black arrows) with methane emissions via sediment redistribution include seasonal indicator draw_area and sub-daily indicators ramp_area, and scour_rate. Douglas Reservoir is a tributary reservoir that feeds into Watts Bar, which is upstream of Guntersville on the mainstem Tennessee River. Vertical bars roughly delimit the period of summer full pool. Boxes enclose the 25th–75th quartile, a horizontal bar denotes the median among years and vertical bars extending to the 5th and 95th percentiles. Outliers are omitted for clarity.

5. Discussion

We developed ICAs to quantify emission risk via four different causal pathways associated with water-level fluctuations (water column, wet-dry cycles, sediment delivery and redistribution, and vegetation). Because they can be simulated from readily available flow, temperature, and bathymetry data, our indicators have practical value to estimate emission risks for reservoirs of different shapes, operation regimes, and climate conditions.

5.1. Longitudinal patterns

Our analysis suggested some interesting longitudinal patterns, some of which compare well with studies of emissions from these reservoirs. Rates of diffusion and ebullition increased downstream from Douglas Reservoir to Guntersville (Bevelhimer et al., 2016). A recent study, showed the same ranking for diffusion, but ebullition was lower in Watts Bar than Douglas (Pilla et al., 2025). These measured emissions did not distinguish among causal pathways or measure emissions mediated by vegetation.

If we assume that emissions via the wet-dry cycle pathway are ebullitive, then our results are consistent with measurements. ICAs suggested a higher potential for methane emission driven by sub-daily water level fluctuations (e.g., via ebullition) downstream in Watts Bar and Guntersville reservoirs than in Douglas reservoir. This reflects the larger perimeter area exposed to ramping in the lower mainstem reservoirs and is also consistent with a very high ebullition measured in Guntersville by Pilla et al. (2025).

Comparing other pathways is more challenging. Along the sediment pathway, results for the seasonal ICA *draw_area,* increased downstream, consistent with field surveys, but not those for the two sub-daily indicators. Resolving the net effect would require field studies to compare the erosional effects of seasonal drawdown versus within-day ramping. To verify longitudinal patterns in the field would require measuring erosion rather than deposition because the latter is affected by trapping in upstream reservoirs (Liu et al., 2016). Along the water-column pathway, lower values of *ramp_vol_frac* (higher emissions) occurred in the upstream tributary reservoir in summer.

ICAs of methane production and consumption both increased downstream. The thermal opportunity for methanogenesis (indicated by *ch4_prod*) was lowest in the tributary reservoir and higher in mainstem reservoirs, as was potential for consumption (indicated by *draw_dur*). This suggests that summer production may be offset by prolonged oxic conditions in the drawdown zone during seasonal drawdown in downstream reservoirs. The net effect on emissions can be evaluated by studies of sediment concentrations, microbial communities, and emissions in the drawdown zone over an annual cycle (Beaulieu et al., 2018; Su et al., 2024).

An interesting side note regarding the vegetation pathway. A recent study suggests that 6 to 20 % of organic carbon produced by macrophytes is buried, a causal pathway not considered here. Accounting for carbon burial in littoral zones produces a threshold; when littoral zones

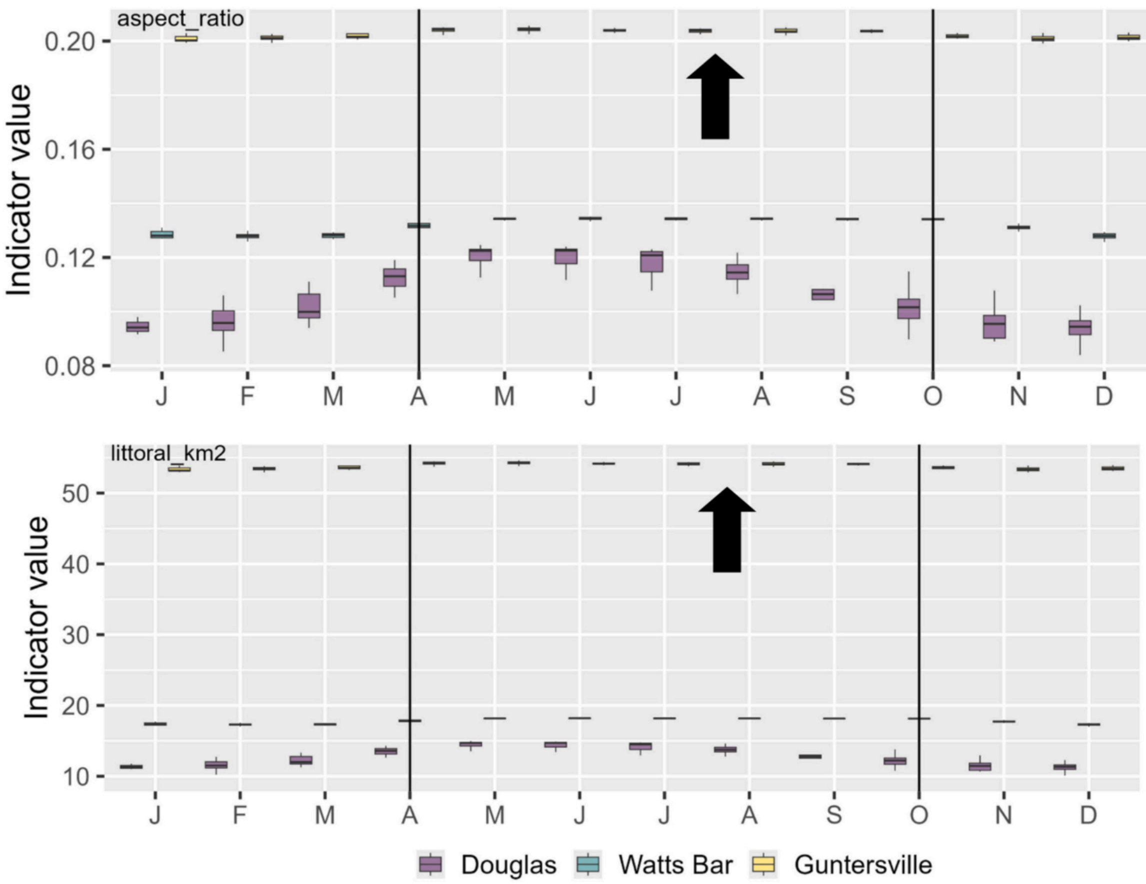

Fig. 9. Sub-daily indicators hypothesized to have a positive relationship (black arrows) with methane emissions via diffusion from littoral vegetation. Douglas Reservoir is a tributary reservoir that feeds into Watts Bar, which is upstream of Guntersville on the mainstem Tennessee River. Heavy vertical bars roughly delimit the period of summer full pool. Box plots show a box enclosing the 25th–75th quartile, a horizontal bar denoting the median and vertical bars extending to the 5th and 95th percentiles. Outliers are omitted for clarity.

exceed 19 % of reservoir area, they become net carbon sinks (Grasset et al., 2025). Here, Guntersville Reservoir is the only reservoir with an *aspect_ratio* above 19 % but it is very close to the threshold (Fig. 9).

5.2. Seasonal patterns

In addition to the longitudinal pattern, ICA's revealed seasonal patterns for some causal pathways. Along the water-column mixing pathway, only one reservoir showed strong seasonal patterns in *ramp_vol_frac*. Douglas Reservoir experienced higher mixing in late summer, which we hypothesize has a net negative effect on methane emissions by oxygenating deeper water. Along the drying-rewetting cycles pathway, indicators measuring the risk of ebullition tended to be higher in summer and fall than in spring.

ICAs with seasonal patterns can inform reservoir management decisions. Specifically, reservoirs and months with higher potential risk of ebullition during drawdown events can be identified by comparing ICAs that measure fast drawdown (*efall_rate*) and high production potential (*ch4_prod*). To illustrate, Watts Bar Reservoir has an intermediate production index and a high *efall_rate* in November, suggesting that operational changes to reduce ebullition events (e.g., by delaying drawdown or restricting ramping rates) might be more effective here than in other reservoirs at key times when methane has accumulated over summer.

5.3. Future directions

Indicators support other components of global greenhouse gas assessments (Forster et al., 2025), but not reservoir emissions. The IPCC approach applies country-specific emissions factors (per unit area) for diffusive and bubble (ebullitive) methane to the cumulative surface areas of reservoirs inundated more than 20 years ago (IPCC, 2006). Global estimates have been produced without first understanding important differences among reservoirs (e.g., climate drivers, morphology, longitudinal position, and operation). The ICAs proposed here can refine the IPCC's Tier 2 approach by developing mechanistic, pathway-specific emissions factors that account for such differences. Before this can be done, studies are needed to more thoroughly test our hypotheses about directions of influence between ICAs and methane emissions via different pathways. For mechanistic models, this is called 'validation by parts' (Collins et al., 2024). For example, previous field studies have focused on quantifying specific events, especially those that produce hot spots and/or hot moments (e.g., fall turnover, eutrophic conditions in summer, drawdown) (Beaulieu et al., 2018). Another relevant approach to model-data comparison is to contrast empirical and model patterns along environmental gradients (Jager et al., 2000). Our longitudinal comparison is an example of this.

Structural equation modeling (SEM) is an alternative that can be used to infer unmeasured methane concentrations and emissions of interest. Indicators serve as proxies for unobserved methane concentrations and emissions, called 'latent' variables. A measurement model specifies how these latent variables can be inferred from measured ICAs and exogenous drivers (Kline, 2005). We present preliminary vision for how this might be done in Appendix C section S3. The measurement model includes ICAs that are influenced by each other and by exogenous variables such as temperature, oxycline depth, and water surface elevation (Appendix C. Fig. S3.1). Measuring covariates uniquely

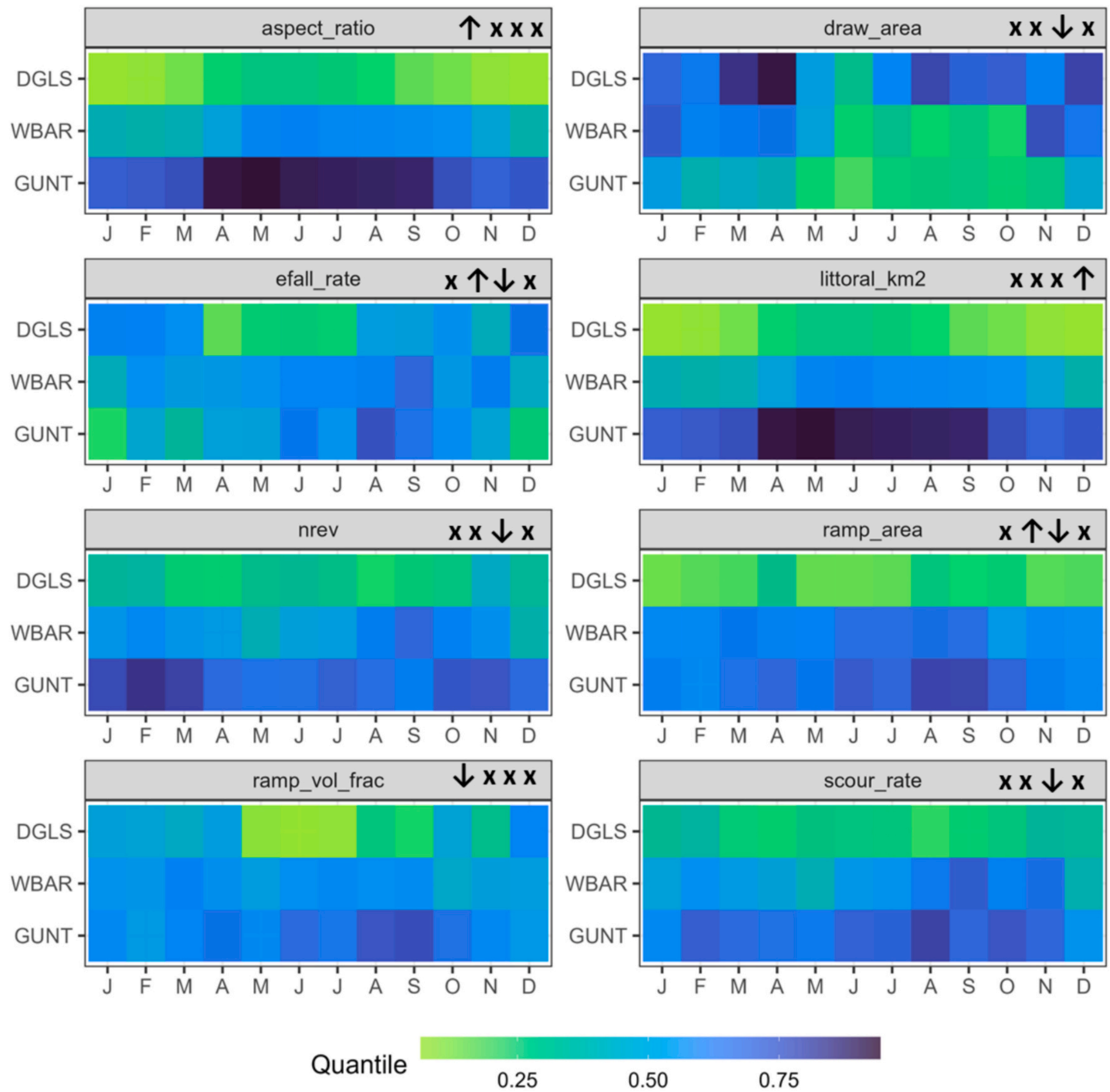

Fig. 10. Heatmaps showing average rank-normalized ICA values by month and reservoir. Rank-normalized values are quantiles relative to all ICA values (water years, months, and reservoirs). Arrows in facets show direction of influence on methane emissions for four pathways (water-column, dry-wetting cycles, sediment, and vegetation).

associated with the four causal pathways can help to distinguish their effects on latent variables (Wang, 2022).

One goal of this study was to develop mechanistic ICAs that would inform reservoir management by estimating emissions associated with changes in water elevation. We identified one example of how ICAs could be combined to inform the timing reservoir releases to minimize ebullitive emissions, either by delaying drawdown or controlling ramping rates at key times. Future research, following the lead of (Marcon et al., 2024), can build on our work by incorporating ICA's related to sediment concentrations, temperature, and oxic conditions (see S3).

CRediT authorship contribution statement

H.I. Jager: Writing – review & editing, Writing – original draft, Visualization, Software, Methodology, Investigation, Formal analysis, Data curation, Conceptualization. **R.M. Pilla:** Writing – review & editing, Visualization, Investigation, Data curation. **A. Cardall:** Formal analysis, Data curation. **C.H. Hansen:** Writing – review & editing, Methodology, Data curation. **P.G. Matson:** Writing – review & editing, Writing – original draft, Visualization. **N.A. Griffiths:** Writing – review & editing, Writing – original draft, Supervision, Resources, Funding acquisition.

Funding

This research was supported in part by the U.S. Department of Energy (DOE), Office of Energy Efficiency and Renewable Energy, Water Power Technologies Office.

Declaration of competing interest

The authors declare that they have no known competing financial interests or personal relationships that could have appeared to influence the work reported in this paper.

Acknowledgements

We appreciate the dam release and elevation data provided by Dr. Stephen Signore, Tennessee Valley Authority. This manuscript has been authored by UT-Battelle, LLC under Contract No. DE-AC05-00OR22725 with the U.S. Department of Energy (DOE). The U.S. Government retains and the publisher, by accepting the article for publication, acknowledges that the U.S. Government retains a non-exclusive, paid-up, irrevocable, world-wide license to publish or reproduce the published form of this manuscript, or allow others to do so, for U.S. Government purposes. The DOE will provide public access to these results of federally sponsored research in accordance with the DOE Public Access Plan (http://energy.gov/downloads/doe-public-access-plan).

Appendix A. Overview of reservoir characteristics

Table A.1
Parameters for selected hydropower reservoirs in the Southeastern US. GRanD data from (Lehner et al., 2011). Calculated summary statistics are at full pool unless otherwise noted, for water years 2006–2019. Photic zone measures sediment perimeter area between full pool and Secchi depth.

Parameter	Douglas	Watts bar	Guntersville
GRanD id	1781	1797	1847
Dam longitude	−83.5346	−84.7830	−86.3921
Dam latitude	35.9638	35.6288	34.4221
Year dam was completed	1943	1942	1939
Storage capacity (cubic km)	1.3346	0.4675	0.2000
Summer net dependable power (MW)	182	196	123
Shoreline (km)	825.6	1162.0	1432.3
Elevation at full pool (m asl)	303.0	225.6	181.3
Elevation at drawdown (m asl)	289.5	224.1	180.7
Refill period	Mar 1 to May 15	Apr 1 to May 15	Apr 1 to Apr 17
Drawdown period	Sep 3 to Dec 30	Nov 1 to Nov 30	Sep 3 to Dec 1
Light extinction coefficient, k_d	1.340	1.027	0.975
Secchi depth (m)	2.278	1.745	1.657
Perimeter, full pool (km)	771.2	879.7	1305.9
GRanD max. depth (m)	29.4	12.0	7.8
Dam height (m)	61.26	34	29
Mean length (km)	36.6	48.1	48.9
Mean width (km)	2.3	3.2	4.4
Photic zone (km^2)	1.591	1.478	2.768

Table A.2
Regression relationships for water surface area as a function of depth, relative to full pool elevation and ramp area as a function of water surface elevation. All parameter estimates were significant at $p \leq 0.1$.

Response	Parameter	Douglas	Guntersville	Watts Bar
Surface area (km^2)	Intercept	118.965	255.561	137.683
	Depth (m)	−7.4415	−35.1325	−11.3617
	Depth^2	0.12312	1.1417	0.22996
	Adjusted R^2	0.9927	0.9625	0.9896
Ramp area (km)	Intercept	−1320	−1102	−1146
	Elevation (m)	9.384	13.34	11.15
	Elevation^2	−0.016	−0.040	−0.0269
	Adjusted R^2	0.9995	0.981	0.9977

Appendix B. Imputation of water surface elevations

Water-surface elevation data was missing for 17 % of 15-min intervals during 2 of the 20 years (2011 and 2012) for Douglas and Watts Bar reservoirs. Missing values in the time series were imputed as follows: For vector $\boldsymbol{Z}$, let $\sum_t z_t$ be the cumulative value at time interval t and $\boldsymbol{I}$ be an indicator variable allowing us to generate cumulative counts of non-missing values. Specifying N as the number of time intervals over which to average (4 15-min periods for sub-daily ICAs), the imputed value at missing time $t0$ is given below.

$$\widehat{z}_{t0} = \frac{\sum_{t0} I_t z_t - \sum_{(t0-N)} I_t z_t}{1 + \sum_{t0} I_t - \sum_{(t0-N)} I_t},$$

$$\text{where } I_t = \begin{cases} 1, z_t \textit{ not missing} \\ 0, z_t \textit{ missing} \end{cases}$$

Appendix C. Supplementary data

Supplementary data to this article can be found online at https://doi.org/10.1016/j.scitotenv.2025.180565.

Data availability

Calculations were performed by using the R Statistical Software v4.3–4.4 (R Core Team, 2024). Code can be found at https://github.com/hjager/GHG-indicators.

References

Aben, R.C.H., Barros, N., van Donk, E., Frenken, T., Hilt, S., Kazanjian, G., et al., 2017. Cross continental increase in methane ebullition under climate change. Nat. Commun. 8.

Beaulieu, J.J., Balz, D.A., Birchfield, M.K., Harrison, J.A., Nietch, C.T., Platz, M.C., et al., 2018. Effects of an experimental water-level drawdown on methane emissions from a eutrophic reservoir. Ecosystems 21, 657–674.

Beaulieu, J.J., Waldo, S., Balz, D.A., Barnett, W., Hall, A., Platz, M.C., et al., 2020. Methane and carbon dioxide emissions from reservoirs: controls and upscaling. J. Geophys. Res. Biogeosci. 125.

Bevelhimer, M., Stewart, A., Fortner, A., Phillips, J., Mosher, J., 2016. CO2 is dominant greenhouse gas emitted from six hydropower reservoirs in the southeastern United States during peak summer emissions. Water 8, 15.

Boavida, I., Diaz-Redondo, M., Fuentes-Perez, J.F., Hayes, D.S., Jesus, J., Moreira, M., et al., 2020. Ecohydraulics of river flow alterations and impacts on freshwater fish. Limnetica 39, 213–232.

Bodmer, P., Vroom, R.J.E., Stepina, T., Del Giorgio, P.A., Kosten, S., 2024. Methane dynamics in vegetated habitats in inland waters: quantification, regulation, and global significance. Front. Water 5.

Collins, A., Koehler, M., Lynch, C., 2024. Methods that support the validation of agent-based models: an overview and discussion. J. Artif. Soc. Soc. Simul. 27, 11.

Deemer, B.R., Harrison, J.A., 2019. Summer redox dynamics in a eutrophic reservoir and sensitivity to a summer's end drawdown event. Ecosystems 22, 1618–1632.

Encinas Fernández, J., Peeters, F., Hofmann, H., 2016. On the methane paradox: transport from shallow water zones rather than in situ methanogenesis is the major source of CH4 in the open surface water of lakes. J. Geophys. Res. Biogeosci. 121, 2717–2726.

Eng, K., Grantham, T.E., Carlisle, D.M., Wolock, D.M., 2017. Predictability and selection of hydrologic metrics in riverine ecohydrology. Freshw. Sci. 36, 915–926.

Fan, L., Dippold, M.A., Thiel, V., Ge, T., Wu, J., Kuzyakov, Y., et al., 2022. Temperature sensitivity of anaerobic methane oxidation versus methanogenesis in paddy soil: implications for the CH 4 balance under global warming. Glob. Chang. Biol. 28, 654–664.

Felix-Faure, J., Walter, C., Balesdent, J., Chanudet, V., Avrillier, J.N., Hossann, C., et al., 2019. Soils drowned in water impoundments: a new frontier. Front. Environ. Sci. 7, 53.

Forster, P.M., Smith, C., Walsh, T., Lamb, W.F., Lamboll, R., Cassou, C., et al., 2025. Indicators of global climate change 2024: annual update of key indicators of the state of the climate system and human influence. Earth Syst. Sci. Data 17, 2641–2680.

Grasset, C., Mesman, J.P., Tranvik, L.J., Maranger, R., Sobek, S., 2025. Contribution of lake littoral zones to the continental carbon budget. Nat. Geosci. 18, 747–752.

Guérin, F., Deshmukh, C., Labat, D., Pighini, S., Vongkhamsao, A., Guédant, P., et al., 2016. Effect of sporadic destratification, seasonal overturn, and artificial mixing on CH4 emissions from a subtropical hydroelectric reservoir. Biogeosciences 13, 3647–3663.

Hansen, C., Pilla, R., Matson, P., Skinner, B., Griffiths, N., Jager, H., 2022. Variability in modelled reservoir greenhouse gas emissions: comparison of select US hydropower reservoirs against global estimates. Environ. Res. Commun. 4, 121008.

Hansen, C.H., Iftikhar, B., Pilla, R.M., Griffiths, N.A., Matson, P.G., Jager, H.I., 2025. Temporal variability in reservoir surface area is an important source of uncertainty in GHG emission estimates. Water Resour. Res. 61, e2024WR037726.

Hao, Q.J., Chen, S.J., Ni, X., Li, X.X., He, X.H., Jiang, C.S., 2019. Methane and nitrous oxide emissions from the drawdown areas of the three gorges reservoir. Sci. Total Environ. 660, 567–576.

Harrison, J.A., Deemer, B.R., Birchfield, M.K., O'Malley, M.T., 2017. Reservoir water-level drawdowns accelerate and amplify methane emission. Environ. Sci. Technol. 51, 1267–1277.

Heink, U., Kowarik, I., 2010. What are indicators? On the definition of indicators in ecology and environmental planning. Ecol. Indic. 10, 584–593.

Hilgert, S., Fernandes, C.V.S., Fuchs, S., 2019. Redistribution of methane emission hot spots under drawdown conditions. Sci. Total Environ. 646, 958–971.

Homa, E.S., Brown, C., McGarigal, K., Compton, B.W., Jackson, S.D., 2013. Estimating hydrologic alteration from basin characteristics in Massachusetts. J. Hydrol. 503, 196–208.

IPCC, 2006. 2006 Guidelines for National Greenhouse gas Inventories. Institute for Global Environmental Strategies, Japan.

Jager, H.I., Hargrove, W.W., Brandt, C.C., King, A.W., Olson, R.J., Scurlock, J.M.O., et al., 2000. Constructive contrasts between modeled and measured climate responses over a regional scale. Ecosystems 3, 396–411.

Jager, H.I., Griffiths, N.A., Hansen, C.H., King, A.W., Matson, P.G., Singh, D., et al., 2022. Getting lost tracking the carbon footprint of hydropower. Renew. Sust. Energ. Rev. 162.

Jager, H.I., Pilla, R.M., Hansen, C.H., Matson, P.G., Iftikhar, B., Griffiths, N.A., 2023. Understanding how reservoir operations influence methane emissions: a conceptual model. Water 15.

Jumani, S., Rao, S., Kelkar, N., Machado, S., Krishnaswamy, J., Vaidyanathan, S., 2018. Fish community responses to stream flow alterations and habitat modifications by small hydropower projects in the Western Ghats biodiversity hotspot. India. Aquat. Conserv.: Mar. Freshw. Ecosyst. 28, 979–993.

Kaczmarek, H., Tyszkowski, S., Habel, M., 2025. Evolution of a reservoir shore zone: geomorphological and ecological responses to water-level fluctuations. Ecol. Indic. 178, 114059.

Keller, P.S., Marcé, R., Obrador, B., Koschorreck, M., 2021. Global carbon budget of reservoirs is overturned by the quantification of drawdown areas. Nat. Geosci. 14, 402–408.

Kennedy, R.H., Thornton, K.W., Ford, D.E., 1985. Characterization of the reservoir ecosystem. In: Gunnison, D. (Ed.), Microbial Processes in Reservoirs, 27. Springer, Dordrecht, The Netherlands, pp. 27–38.

Kline, R.B., 2005. Principles and Practices of Structural Equation Modeling. The Guilford Press, New York.

Laura, E.J., Kurtz, J.C., Fisher, W.S., 2000. Evaluation Guidelines for Ecological Indicators. U.S. Environmental Protection Agency, Research Triangle Park, NC, p. 107.

Lehner, B., Liermann, C.R., Revenga, C., Vorosmarty, C., Fekete, B., Crouzet, P., et al., 2011. High-resolution mapping of the world's reservoirs and dams for sustainable river-flow management. Front. Ecol. Environ. 9, 494–502.

Liu, S., Lu, X.X., Xia, X., Zhang, S., Ran, L., Yang, X., et al., 2016. Dynamic biogeochemical controls on river pCO2 and recent changes under aggravating river impoundment: an example of the subtropical Yangtze River. Glob. Biogeochem. Cycles 30, 880–897.

Liu, L., Yang, Z.J., Delwiche, K., Long, L.H., Liu, J., Liu, D.F., et al., 2020. Spatial and temporal variability of methane emissions from cascading reservoirs in the upper Mekong River. Water Res. 186, 116319.

Lyautey, E., Billard, E., Tissot, N., Jacquet, S., Domaizon, I., 2021. Seasonal dynamics of abundance, structure, and diversity of methanogens and Methanotrophs in Lake sediments. Microb. Ecol. 82, 559–571.

Maavara, T., Chen, Q., Van Meter, K., Brown, L.E., Zhang, J., Ni, J., et al., 2020. River dam impacts on biogeochemical cycling. Nat. Rev. Earth Environ. 1, 103–116.

Marcon, L., Bleninger, T., Männich, M., Ishikawa, M., Hilgert, S., Lorke, A., 2024. Exploring the temporal dynamics of methane ebullition in a subtropical freshwater reservoir. PLoS One 19, e0298186.

McManamay, R.A., George, R., Morrison, R.R., Ruddell, B.L., 2022. Mapping hydrologic alteration and ecological consequences in stream reaches of the conterminous United States. Sci. Data 9.

Nzotungicimpaye, C.-M., Zickfeld, K., Macdougall, A.H., Melton, J.R., Treat, C.C., Eby, M., et al., 2021. WETMETH 1.0: a new wetland methane model for implementation in earth system models. Geosci. Model Dev. 14, 6215–6240.

Pierangeli, G.M.F., Domingues, M.R., Jesus, T.A.D., Coelho, L.H.G., Hanisch, W.S., Pompêo, M.L.M., et al., 2021. Higher abundance of sediment methanogens and methanotrophs do not predict the atmospheric methane and carbon dioxide flows in eutrophic tropical freshwater reservoirs. Front. Microbiol. 12.

Pilla, R.M., Griffiths, N.A., Hansen, C., Turner, D., Fortner, A.M., Trent Jett, R., et al., 2025. Comparison of greenhouse gas emission estimates from six hydropower reservoirs using modeling versus field surveys. Biogeochemistry 168, 28.

Prairie, Y.T., Alm, J., Beaulieu, J., Barros, N., Battin, T., Cole, J., et al., 2018. Greenhouse gas emissions from freshwater reservoirs: what does the atmosphere see? Ecosystems 21, 1058–1071.

R Core Team, 2024. R: A Language and Environment for Statistical Computing. R Foundation for Statistical Computing, Vienna, Austria.

Rey-Sanchez, C., Bohrer, G., Slater, J., Li, Y.F., Grau-Andrés, R., Hao, Y., et al., 2019. The ratio of methanogens to methanotrophs and water-level dynamics drive methane transfer velocity in a temperate kettle-hole peat bog. Biogeosciences 16, 3207–3231.

Richter, B.D., Baumgartner, J.V., Powell, J., Braun, D.P., 1996. A method for assessing hydrologic alteration within ecosystems. Conserv. Biol. 10, 1163–1174.

Rodriguez, M., Gonsiorczyk, T., Casper, P., 2018. Methane production increases with warming and carbon additions to incubated sediments from a semiarid reservoir. Inland Waters 8, 109–121.

Saunois, M., Bousquet, P., Poulter, B., Peregon, A., Ciais, P., Canadell, J.G., et al., 2016. The global methane budget 2000-2012. Earth Syst. Sci. 8, 697–751.

Schindler, D.W., 1971. Light, temperature, and oxygen regimes of selected lakes in the Experimental Lakes area, northwestern Ontario. J. Fish. Res. Board Can. 28, 157–169.

Soued, C., Harrison, J.A., Mercier-Blais, S., Prairie, Y.T., 2022. Reservoir CO2 and CH4 emissions and their climate impact over the period 1900–2060. Nat. Geosci. 15, 700–705.

Steyaert, J.C., Condon, L.E., S, W.D.T., Voisin, N., 2022. ResOpsUS, a dataset of historical reservoir operations in the contiguous United States. Sci. Data 9, 34.

Su, Y., Liu, W., Rahaman, M.H., Chen, Z., Zhai, J., 2024. Methane emission from water level fluctuation zone of the three gorges reservoir: seasonal variation and microbial mechanism. Sci. Total Environ. 912, 168935.

Tennessee Valley Authority, 2004. Tennessee Valley authority reservoir operations study. In: Shipp, L.B. (Ed.), Programmatic Environmental Impact Statement. Tennessee Valley Authority, Knoxville, TN, p. 118.

Thalasso, F., Sepulveda-Jauregui, A., Gandois, L., Martinez-Cruz, K., Gerardo-Nieto, O., Astorga-España, M.S., et al., 2020. Sub-oxycline methane oxidation can fully uptake CH4 produced in sediments: case study of a lake in Siberia. Sci. Rep. 10.

Thornton, M.M., Shrestha, R., Wei, Y., Thornton, P.E., Kao, S.C., 2022. Daymet: Daily Surface Weather Data on a 1-Km Grid for North America, Version 4 R1. ORNL Distributed Active Archive Center.

Tian, W., Wang, H., Xiang, X., Loni Prakash, C., Qiu, X., Wang, R., et al., 2023. Water table level controls methanogenic and methanotrophic communities and methane emissions in a Sphagnum-dominated peatland. Microbiol. Spectr. 11, e01992-23.

Wang, Z., 2022. A comparison of three approaches to covariate effects on latent factors. Large-Scale Assess. Educ. 10, 26.
Wang, G.S., Jager, H.I., Baskaran, L.M., Brandt, C.C., 2018. Hydrologic and water quality responses to biomass production in the Tennessee river basin. Glob. Change Biol. Bioenergy. 10, 877–893.
Wetzel, R.G., 1983. Limnology. Saunders College Publishing, Philadelphia, PA, USA.
Zhong, J., Yang, F., Zhang, M., Sun, C., Wang, S., Chen, Q., et al., 2023. Water depth and productivity regulate methane (CH4) emissions from temperate cascade reservoirs in northern China. J. Hydrol. 626, 130170.